Biochimica et Biophysica Acta 1863 (2016) 596–606

Contents lists available at ScienceDirect

Biochimica et Biophysica Acta

journal homepage: www.elsevier.com/locate/bbamcr

Clock genes-dependent acetylation of complex I sets rhythmic activity of mitochondrial OxPhos

Olga Cela [a,1], Rosella Scrima [a,1], Valerio Pazienza [b], Giuseppe Merla [c], Giorgia Benegiamo [b,2], Bartolomeo Augello [c], Sabino Fugetto [a], Marta Menga [a], Rosa Rubino [d], Luise Fuhr [e,f], Angela Relógio [e,f], Claudia Piccoli [a], Gianluigi Mazzoccoli [d,*], Nazzareno Capitanio [a,**]

[a] Department of Clinical and Experimental Medicine, University of Foggia, Foggia, Italy
[b] Gastroenterology Unit, IRCCS "Casa Sollievo della Sofferenza", San Giovanni Rotondo (FG), Italy
[c] Medical Genetics Unit, IRCCS "Casa Sollievo della Sofferenza", San Giovanni Rotondo (FG), Italy
[d] Department of Medical Sciences, Division of Internal Medicine and Chronobiology Unit, IRCCS "Casa Sollievo della Sofferenza", San Giovanni Rotondo (FG), Italy
[e] Institute for Theoretical Biology (ITB), Charité-Universitätsmedizin Berlin and Humboldt-Universität zu Berlin, Berlin, Germany
[f] Molekulares Krebsforschungszentrum (MKFZ), Charité-Universitätsmedizin Berlin, Berlin, Germany

ARTICLE INFO

Article history:
Received 12 June 2015
Received in revised form 30 November 2015
Accepted 23 December 2015
Available online 28 December 2015

Keywords:
Mitochondria
Clock-genes
Oxidative phosphorylation
Complex I
NAD
Sirtuins

ABSTRACT

Physiology of living beings show circadian rhythms entrained by a central timekeeper present in the hypothalamic suprachiasmatic nuclei. Nevertheless, virtually all peripheral tissues hold autonomous molecular oscillators constituted essentially by circuits of gene expression that are organized in negative and positive feed-back loops. Accumulating evidence reveals that cell metabolism is rhythmically controlled by cell-intrinsic molecular clocks and the specific pathways involved are being elucidated. Here, we show that in vitro-synchronized cultured cells exhibit BMAL1-dependent oscillation in mitochondrial respiratory activity, which occurs irrespective of the cell type tested, the protocol of synchronization used and the carbon source in the medium. We demonstrate that the rhythmic respiratory activity is associated to oscillation in cellular NAD content and clock-genes-dependent expression of NAMPT and Sirtuins 1/3 and is traceable back to the reversible acetylation of a single subunit of the mitochondrial respiratory chain Complex I. Our findings provide evidence for a new interlocked transcriptional-enzymatic feedback loop controlling the molecular interplay between cellular bioenergetics and the molecular clockwork.

1. Introduction

In mammals many physiological processes display circadian rhythmicity in response to external oscillating stimuli (light/darkness, feeding/fasting and temperature cycles) or internal endocrine secretion [1]. The main pacemaker controlling the diurnal rhythms is represented by the suprachiasmic nuclei (SCN), which are located in the hypothalamus and receive photic inputs from the retina through the retinohypothalamic tract. The molecular basis of the pacemaker activity of the SCN relays on a relatively low number of clock genes, which act by transcriptional-translational auto-regulatory feedback loops [2].

The negative limb of the loop is operated by the transcriptional activators CLOCK and BMAL1 and their target genes Period (*PER*) and Cryptochrome (*CRY*), which encode circadian proteins accumulating and forming a repressor complex that interacts with CLOCK-BMAL1 heterodimers to inhibit their transcriptional activity. The orphan nuclear hormone receptors REV-ERBα and RORα operate a feedback loop controlling negatively and positively *BMAL1* transcription, respectively [3].

Accumulating evidences support the notion that the cells of virtually all the peripheral tissues are endowed with autonomous self-sustained

Abbreviations: Clock, circadian locomotor output cycles kaput; Bmal, brain and muscle aryl hydrocarbon receptor nuclear translocator (ARNT)-like; SNC, suprachiasmic nuclei; PER, period; CRY, cryptochrome; ROR-alpha, RAR-related orphan receptor alpha; NAM, nicotinamide; NAD, nicotinamide adenine dinucleotide; NAMPT, nicotinamide phosphoribosyltransferase; PGC-1α, proliferator-activated receptor gamma coactivator 1-alpha; SIRT, sirtuin (silent mating type information regulation 2 homolog); OxPhos, oxidative phosphorylation; DMEM, Dulbecco's Modified Eagle's Medium; PBS, phosphate-buffered saline; OCR_{RR}, resting oxygen consumption rate; OCR_{OL}, oxygen consumption rate in the presence of oligomycin; OCR_{UNC}, uncoupled oxygen consumption rate; FCCP, carbonilcyanide p-triflouromethoxyphenylhydrazone; $\Delta\Psi_m$, mitochondrial membrane electrical potential; TMRM, tetramethylrhodamine, methyl ester.

* Correspondence to: G. Mazzoccoli, Department of Medical Sciences, Division of Internal Medicine and Chronobiology Unit, IRCCS Scientific Institute and Regional General Hospital "Casa Sollievo della Sofferenza", San Giovanni Rotondo (FG), 71013, Italy.
** Correspondence to: Nazzareno Capitanio, Department of Clinical and Experimental Medicine, University of Foggia, Foggia, Biomedical Pole "E. Altomare", via Napoli, 71122, Italy.
E-mail addresses: g.mazzoccoli@operapadrepio.it (G. Mazzoccoli), nazzareno.capitanio@unifg.it (N. Capitanio).
[1] Equal contribution.
[2] Present address: University of Zurich, Institute of Pharmacology and Toxicology, Chronobiology and Sleep Research Unit, Winterthurerstrasse 190, CH-8057 Zurich, Switzerland.

http://dx.doi.org/10.1016/j.bbamcr.2015.12.018
0167-4889/

molecular oscillators constituted by the same clock gene machinery operating in the SCN. The function of the SCN, therefore, is to receive the light signals and entrain the phases of the peripheral oscillators [4]. Noticeably, recent evidences show that about half of all protein coding genes in mammals displays circadian transcription rhythms largely in an organ-specific manner [5].

The amplitude of oscillation of many clock genes is influenced by SIRT1, a type III histone/protein deacetylase [6]. The activity of SIRT1 depends on the oscillating levels of nicotinamide (NAM) adenine dinucleotide (NAD), synthesized in the salvage pathway by the committing nicotinamide phosphoribosyltransferase (NAMPT), whose expression shows a circadian rhythm [7,8].

Importantly, peroxisome proliferator-activated receptor gamma coactivator 1-alpha (PGC-1α), a master transcriptional coactivator positively controlling mitochondrial biogenesis and redox homeostasis [9] proved to be a target of SIRT1 thereby providing support for a reciprocal interaction between metabolism and the circadian clock [10,11]. Consistently, recent studies have addressed the role that mitochondrial bioenergetics and dynamics play in cell metabolism in relation to circadian rhythmicity [8,12,13]. Such data highlights the interplay between mitochondrial oxidative phosphorylation (OxPhos) and the functioning of the biological clock, fostering further in-depth analysis.

Aim of the present study was to investigate the mutual impact of circadian clock gene oscillation and the mitochondrial respiratory activity taking advantage of a well established in vitro model of synchronized cultured human cells.

2. Materials and methods

2.1. Cell culture and "in vitro" synchronization protocols

HepG2 cells were obtained from the European Collection of Cell Cultures (ECACC Salisbury, UK). Cell cultures were maintained at 37 °C in the presence of 5% CO_2 in DMEM (low-glucose) supplemented with 10 mM Hepes, 10% inactivated fetal bovine serum (FBS), 2 mM glutamine, 100 U/ml of penicillin and 100 μg/ml of streptomycin. The serum shock induced synchronization was performed as in [14,15]. Briefly: approximately 3×10^6 cells/dish were plated the day before the experiments. At the day of the experiments, culture medium was exchanged with serum-rich DMEM, containing 50% FBS, for 2 h and then the medium was replaced with serum-free DMEM. Alternatively, HepG2 cells were synchronized by incubation with 0.1 μM dexamethasone (directly added to the culturing medium) for 15 min; thereafter dexamethasone was washed-out by replenishing HepG2 cells with DMEM (+10% FBS) [16]. The cells were harvested and assayed at the different time points indicated in the text/figures. Cell cultures were typically utilized at a passage number below 18–20 and at a confluence of 80–85%.

2.2. Quantitative RT-PCR

Total RNA from HepG2 at different time points was extracted using the RNeasy® Mini Kit (Qiagen S.p.a. Milan, Italy) and subsequently digested by DNase I. cDNA was synthesized from 100 ng total RNA with Quantifast RT-PCR kit (Qiagen). For real-time PCR, we used the following SYBR Green QuantiTect Primers purchased from Qiagen: REVERBα (QT00000413), RORα (QT00072380), ARNTL (QT00068250), ARNTL2 (QT00011844), CLOCK (QT00054481), PER1 (QT00069265), PER2 (QT00011207), PER3 (QT00097713), CRY1 (QT00025067), CRY2 (QT00094920), NAMPT (QT00087920), SIRT1 (QT00051261), SIRT3 (QT00091490) and PPARGC1A (QT00095578). Reactions were set up in 96-well plates using a 7700 Real-Time PCR System (Applied Biosystems, Foster City, CA, USA). Expression levels of the target gene were normalized using the housekeeping control gene TATA binding protein (TBP, QT00000721). mRNA amount of each target gene relative to TBP was calculated through the comparative Ct method (i.e. the $2^{(-\Delta\Delta Ct)}$ method).

2.3. Real time luminescence measuring

Stable-transduced cell populations were selected and maintained in medium containing hygromycin B (100 μg/ml, Gibco). For live-cell bioluminescence recording, cells were maintained in phenol red-free DMEM (Gibco) containing 10% FBS, 1% penicillin-streptomycin and 250 μM D-Luciferin (PJK). Cell morphology and density were controlled by light microscopy. All cells were incubated at 37 °C in a humidified atmosphere with 5% CO_2. Lentiviral elements containing a *Bmal1*-promoter-driven luciferase (BLH) were generated as previously described [17]. HEK293T cells were seeded in 175 cm^2 culture flasks and co-transfected with 12.5 μg packaging plasmid psPAX, 7.5 μg envelope plasmid pMD2G and 17.5 μg *Bmal1*-promoter (BLH)-luciferase expression plasmid using the CalPhos mammalian transfection kit (Clontech) according to the manufacturer's instruction. To harvest the lentiviral particles, the supernatant was centrifuged at 4100 x g for 15 min to remove cell debris and passed through a 45 μm filter (Sarstedt). The lentiviral particles were stored at −80 °C. For lentiviral transduction, 2×10^5 cells were seeded in 6-well plates in 1 ml medium and 1 ml of lentiviral particles was added. 8 μg/ml protamine sulfate (Sigma) was used to enhance transduction efficiency The next day, the medium was replaced with selection medium (complete growth medium containing 100 μg/ml hygromycin B to obtain stable transduced cells and incubated at 37 °C with 5% CO_2 atmosphere. For bioluminescence measurement, 1.2×10^6 cells were plated in 35 mm dishes (Thermo Scientific) one day prior to measurements. Cells were either synchronized by a single pulse of 0.1 μM dexamethasone (Sigma-Aldrich) for 15 min (Dex 1) or 1 μM dexamethasone for 45 min (Dex 2) or by serum shock with medium containing 50% FBS for 2 h (Serum shock). Next, cells were washed once with 1× PBS and phenol-red-free DMEM supplemented with 250 μM D-Luciferin was added. *Bmal1*-promoter-(BLH)-reporter activity was measured, using a LumiCycle instrument (Actimetrics) for 5 days. Raw luminescence data were de-trended by subtracting luminescence counts by the 24 h running average using the LumiCycle software.

2.4. BMAL1-specific siRNA transfection in HepG2 cells

BMAL1-specific siRNA was purchased from Sigma-Aldrich (Mission Pre-designed siRNA2D). HepG2 cells were seeded on 60-mm dishes and at 30–50% confluence were transiently transfected with the BMAL1-specific siRNA diluted in Opti-MEM using Lipofectamine® 2000 Transfection Reagent (Invitrogen) according to the manufacturer's protocol. After 6 h of incubation at 37 °C, the transfection medium was replaced with complete medium containing 10% FBS and The experiments were conducted 12 and 24 h later.

2.5. Respirometric measurements

Cultured cells were gently detached from the dish by tripsinisation, washed in PBS, harvested by centrifugation at 500 ×*g* for 5 min and immediately assessed for O_2 consumption with a high resolution oxymeter (Oxygraph-2 k, Oroboros Instruments). About $8–10 \times 10^6$ viable cells/ml were assayed in DMEM at 37 °C; after attainment of a stationary endogenous substrate-sustained resting oxygen consumption rate (OCR_{RR}), 2 μg/ml of the ATP-synthase inhibitor oligomycin was added (OCR_{OL}) followed by addition of 0.3 μM of the uncoupler carbonilcyanide p-triflouromethoxyphenylhydrazone (FCCP) (OCR_{UNC}). The rates of oxygen consumption were corrected for 2 μM antimycin A + 2 μM rotenone-insensitive respiration. The respiratory control ratio (RCR) was obtained by the ratio OCR_{UNC}/OCR_{OL}, the leak by the ratio OCR_{OL}/OCR_{UNC} and the ATP-synthesis-linked respiration (OxPhos) by the ratio $(OCR_{RR}–OCR_{OL})/OCR_{UNC}$. For measurement of the succinate-

O_2 reductase activity, cells suspended in DMEM were permeabilized with 10 μg digitonin/10^6 cell for 15 min until the OCR was stationary decreased; thereafter, 2 μM rotenone was added and the reaction started with 5 mM succinate. The attained OCR was corrected for 2 μM antimycin A-insensitive respiration and normalized to the initial cell number.

2.6. Flow cytometry and fluorescence microscopy ($\Delta\Psi_m$ analysis)

Flow cytometry. Serum shocked cultured cells were detached after the indicated time by trypsinization, pelleted by centrifugation (500×g, 10 min), resuspended in PBS and incubated with 0.1 μM tetramethylrhodamine, methyl ester (TMRM) for 15 min at 37 °C. Thereafter the stained cells were analyzed without washing by fluorescence-activated cell sorting (FACS) with a EPICS XL MCL flow cytometer (Beckman Coulter Fullerton, CA, USA) (10^4events/run).

Fluorescence microscopy. Cells were seeded in an 8-well chambered cover glass and synchronized by a staggered protocol so to reach at the same time 0,6,12,18 h after serum-shock. Fluorescence microscopy. Cells were washed with phenol red-free DMEM, incubated in the dark for 15 min with 2 μM tetramethylrhodamine, methyl ester (TMRM) at 37 °C and immediately imaged by EVOS® FL Cell Imaging System (60×). At least 10 different optical fields were captured for each sample. Analysis of the digitalized images was performed using ImageJ 1.48u software (http://imagej.nih.gov/ij).

2.7. NAD measurement

Cells, collected by trypsinization, were pelleted, resuspended in 400 μl of extraction buffer (20 mM $NaHCO_3$, 100 mM Na_2CO_3, 10 mM nicotinamide, 0.05% (*v*/*v*) TritonX100, pH 10.3), subjected to two cycles of freeze-thaw and centrifuged at 13,000 ×*g* for 15 min. The resulting supernatant was split in two equal volumes, one for determination of total NAD, the other for determination of NADH following incubation at 60 °C for 30 min. NAD or NADH concentrations were measured in cyclic enzyme reaction system in which alcohol dehydrogenase (ADH) reduces dichlorophenol indolphenol (DCIPIP) through the intermediation of phenazine methosulfate (PMS). The reaction mixture consisted of 380 μl of 5 mM EDTA, 100 mM Tris–HCl (pH 7.5) supplemented with 86 μM DCIPP, 120 μM PMS, 20 U/ml ADH, 2.5% (*v*/*v*) ethanol. The reaction was started by addition of 20 μl of the sample and reduction of the blue-colored DCPIP to colorless $DCPIPH_2$ was measured by recording spectrophotometrically the decrease in absorbance at 600 nm. The concentration of NAD and NADH in each extract was determined by comparing sample values to standard curves (generated from samples containing known amounts of NAD and NADH that had been cycled under identical conditions as the samples) and normalized to the protein concentration of the extracts.

2.8. Measurement of mitochondrial respiratory complexes and citrate synthase activity

The specific activity of NADH: ubiquinone oxidoreductase (complex I) was assayed spectrophotometrically on frozen–thawn and ultrasound-treated cells in 10 mM Tris, 1 mg/ml serum albumin, pH 8.0 (in the presence of 1 μg/ml of antymicin A *plus* 2 mM KCN) by following the initial 2 μg/ml rotenone-sensitive rate of 50 μM NADH oxidation (ε_{340nm} = 6.22 mM^{-1} cm^{-1}) in the presence of 200 μM decylubiquinone (dUQ) as electron acceptor [18]. The activity of the complexes II + III + IV (succinate-O_2 reductase) was measured polarographically as described in Section 2.2; HepG2 cell suspension was supplemented with 20 μg digitonin/10^6 cells and 1 μM rotenone and the succinate-O_2 reductase activity was measured as 0.2 μM antymicin A-sensitive OCR elicited by 5 mM succinate. The activities were normalized to the initial cell number and to cellular protein content. Citrate synthase catalyzes the reaction between acetyl coenzyme A and oxaloacetic acid to form citric acid. Citrate synthase activity was assayed spectrophotometrically (ε_{412nm} = 13.6 mM^{-1} cm^{-1}) measuring the reaction between CoA-SH and DTNB to form 5-thio-2-nitrobenzoic acid (TNB) as in [18].

2.9. Immunoblotting and 2D blue native-SDS PAGE

Total protein extract from 10^7 HepG2 cells was subjected to SDS-PAGE (12% acrylamide) and electroblotted by standard procedures. For BMAL1 and SIRT3 detection rabbit polyclonal Abs (18,986-Abcam, dil. 1:1000 and AB2298-Merck Millipore, 1:5000 respectively) were used and a HRP-conjugated anti-rabbit IgG as secondary Ab (Thermo Scientific, dil. 1:20,000). For the mitochondrial OxPhos omplexes profile a cocktail of mouse mABs recognizing specific subunits of the respiratory chain complex and of the ATP-synthase (MitoProfile® Total OXPHOS (Abcam), 1:700) was used; HRP-conjugated anti-mouse IgG were used as secondary Ab (Thermo Scientific, 1:8000) according to standard procedures and bands visualized by chemiluminescence densitometric analysis (Versadoc Imaging System). *2D Blue Native-SDS PAGE of mitoplast proteins*. Mitochondrial-enriched fractions were obtained from HepG2 cells by differential centrifugation. Briefly, 10^8 cultured cells were harvested (by scraping) in 250 mM sucrose, 1 mM EDTA, 5 mM Hepes, 3 mM $MgCl_2$ (pH 7.4) supplemented with 10 μl/ml of protease inhibitors stock solution (SIGMA) and disrupted by tight teflon-glass homogenization; the homogenate was centrifuged at 1000 ×*g* for 10 min and the resulting supernatant at 14,000 ×*g* for 15 min. The resulting pellet was washed and finally re-suspended in a minimum volume of the same buffer. Blue native-PAGE was performed as described in [19]. The first dimension native electrophoresis was run in a 5–12% acrylamide gradient. Rectangular gel patches including Complex I were excised from each sample lane and placed on a glass plate for incubation with lysis buffer at room temperature. The Complex I subunits were separated by a denaturing Tricine-SDS-PAGE and transferred to nitrocellulose membrane using an immersion electrophoretic transfer cell (Bio-Rad) at 40 V overnight at 4 °C. Acetylated proteins were detected by using mouse anti-acetylated lysine (Abnova, 1:1000) and HPR-conjugated anti-mouse IgC (Thermo Scientific, 1:20,000) as primary and secondary Ab, respectively, according to standard Western blotting procedure and visualized by chemiluminescence densitometric analysis (Versadoc Imaging System).

2.10. Cosinor analysis

The following equation was used to fit the experimental data from 0 to 24–30 h in synchronized cells:

$f(t) = M + A\cos(t2\pi/P + \varphi) + st$; with M = mesor, A = amplitude, P = period, φ = acrophase, s = slope. The best fit was attained using the software GraFit (V 4.0.13, Erithacus Software Limited).

2.11. Statistical analysis

Experimental data are shown as mean ± standard error of the mean (SEM) with "n" indicating the number of independent experiments. Data were compared by an unpaired Student-*t*-test. Differences were considered statistically significant when the P value was less than 0.05. All analyses were performed using Graph Pad Prism (Graph Pad software, San Diego, CA, USA).

3. Results and discussion

3.1. Synchronized cultured cells exhibit autonomous oscillatory rhythm of mitochondrial respiratory activity

We used the well-established serum shock procedure [14,15] to synchronize Hep-G2 cells, which exhibit a high mitochondrial content and efficient OxPhos [20]. Following synchronization, intact cells were

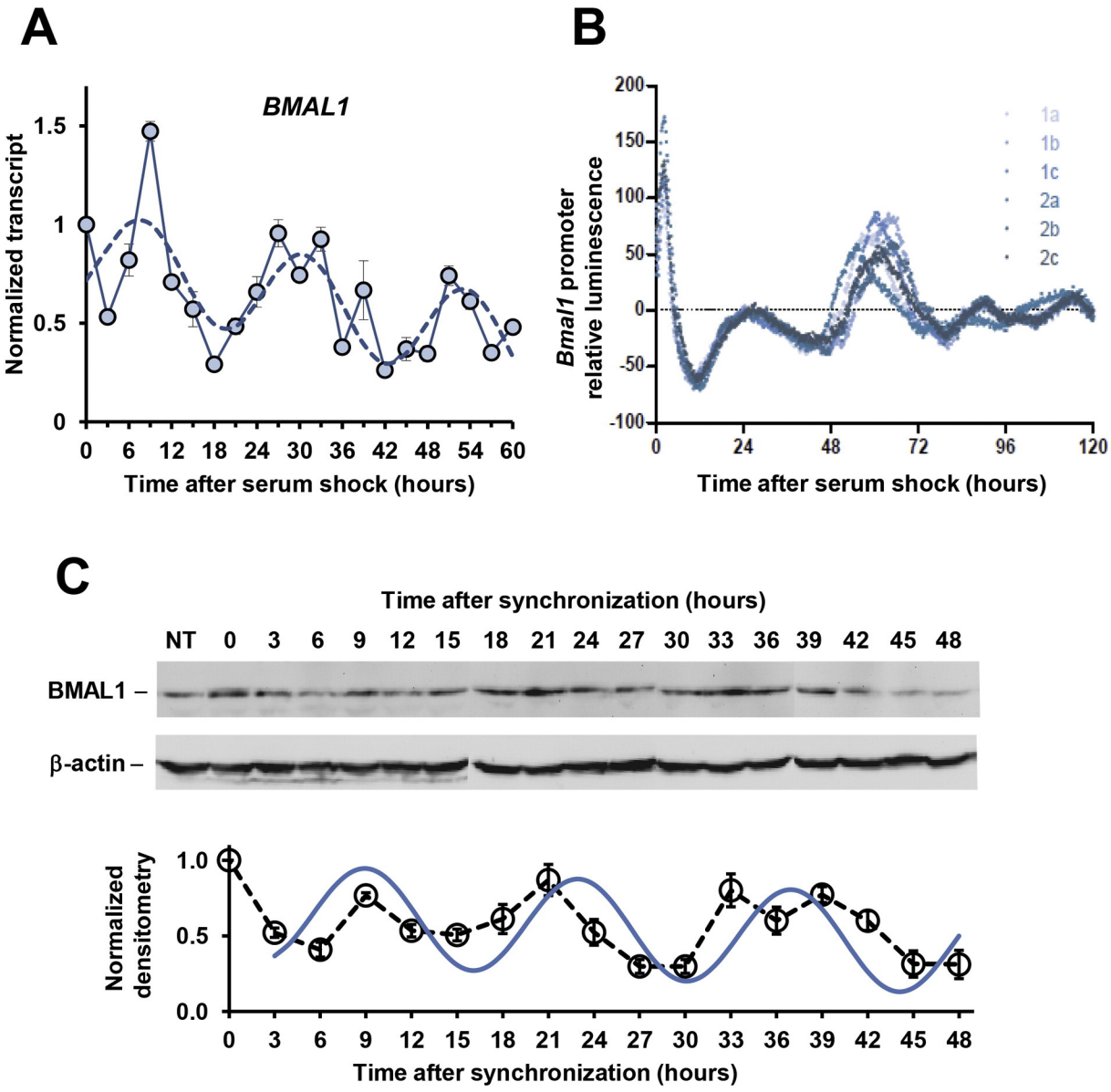

Fig. 1. Analysis of BMAL1 expression in serum shocked synchronized HepG2 cells. A q-RT-PCR assay for *BMAL1* transcript; means ± S.E.M. of 3 independent experiments (n = 3); dashed line, COSINOR best fit. B Bioluminescence measurements of HepG2 cells lentivirally transduced with a *BMAL1*-luciferase construct. Two sets of stably transfected cells were produced and measured in triplicate (1a-c and 2a-c). C Immunoblotting of total cell protein extract toward BMAL1. Upper panel, representative Western blotting; lower graph, densitometric analysis, normalized to b-actin and to ST = 0, showing the average ± S.E.M. of 3 independent experiments; continuous line, COSINOR best fit.

assayed every three hours up to sixty hours. Fig. 1A shows that the transcription of *BMAL1*, a key core clock gene driving circadian rhythms [21], displayed an oscillatory activity, peaking at 9 h post-synchronization (i.e. acrophase) and with a period of 22.7 ± 1.3 h (Cosinor best-fit [22]), thus confirming in HepG2 cells what observed for other cell types [23]. The genes encoding REV-ERBα and ROR-α displayed a similar oscillatory transcriptional profile but with the acrophase at 15 h, consistent with their negative control of BMAL1 expression [1]; conversely the expression of *CLOCK*, *PER1-3* and *CRY1-2* was considerably less pronounced (Supplemental Fig. S1). The clock-gene oscillatory activity was further confirmed in HepG2 cells lentivirally transduced with a *BMAL1* promoter-luciferase construct. Fig. 1B displays the luminescence real-time monitoring of the gene reporter in synchronized cells and shows an oscillatory profile with a period of 28.9 ± 0.3 h characterized by alternation of high and low amplitude peaks over the 5 days of measurement. Intriguingly, immune-detection of the BMAL1 protein in synchronized HepG2 cells resulted, over a period of 48 h, in an oscillatory profile with an acrophase at 9 h but with a period of 11.4 ± 0.7 h (Fig. 1C). The reason of the observed discrepancy between the expression patterns of *BMAL1* mRNA and protein, although deserving further investigation, was out of the aim of this study. A possible explanation might involve a time-dependent differential proteolytic degradation of BMAL1 which is known to be controlled through the AMPK-casein kinase I axis [24,25].

Then intact synchronized Hep-G2 cells were assayed by high-resolution respirometry over a period of 45 h. Fig. 2A shows that the oxygen consumption rate (OCR), sustained by endogenous substrates, under resting conditions (OCR_R) displayed an oscillatory activity with maxima peaking at 12, 27 and 39 h after serum shock. A similar oscillatory pattern was observed for the OCR under uncoupled conditions (OCR_U) or in the presence of oligomycin (OCR_o). Conversely, no oscillatory activity was observed for the OCR insensitive to rotenone plus antimycin A (not shown), thus ruling out changes of the non-mitochondria-related OCR respectively. Noticeably, in the absence of serum shock the amplitude of the respiratory oscillation was markedly damped (Fig. 2A) as well as under conditions of persistent serum load

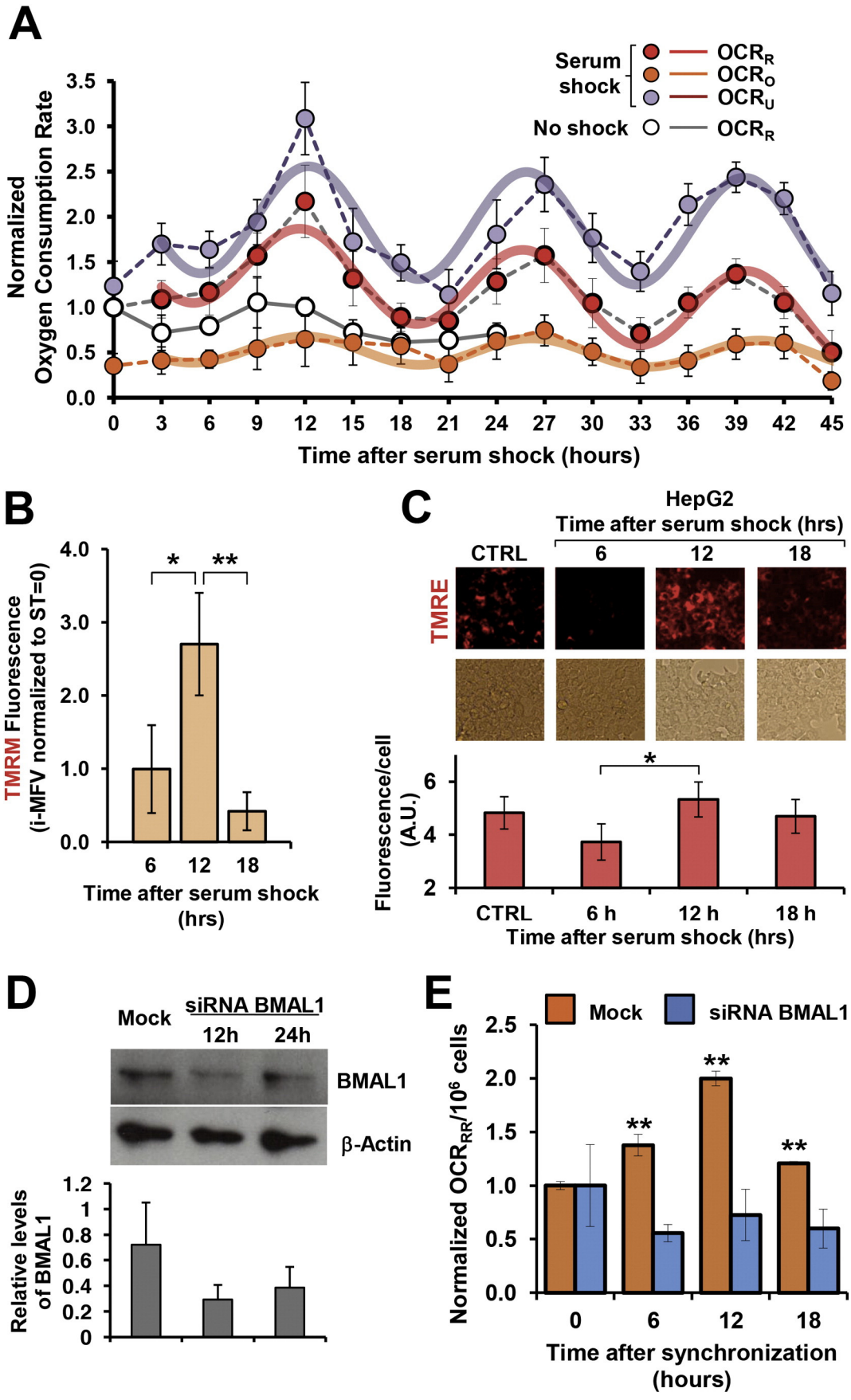
A
Serum shock
OCR_R
OCR_O
OCR_U
No shock
OCR_R
Normalized Oxygen Consumption Rate
Time after serum shock (hours)
B
TMRM Fluorescence (i-MFV normalized to ST=0)
Time after serum shock (hrs)
C
HepG2
Time after serum shock (hrs)
CTRL
6
12
18
TMRE
Fluorescence/cell (A.U.)
CTRL
6 h
12 h
18 h
Time after serum shock (hrs)
D
Mock
siRNA BMAL1
12h
24h
BMAL1
β-Actin
Relative levels of BMAL1
E
Mock
siRNA BMAL1
Normalized OCR_RR/10^6 cells
Time after synchronization (hours)

(data not shown). The amplitude (i.e. the difference between zenith and nadir) of both the $OCR_r - OCR_o$ difference (a measure of the OCR controlled by the ATP synthesis) and the OCR_u/OCR_o ratio (a measure of the OxPhos efficiency) were significantly different in synchronized cells (Fig. S2). Normalization of the OCR to the cell number or protein content was not influential, as the amount of protein *per* cell did not change significantly following synchronization (Fig. S3).

Cosinor analysis of the data points [22] fitted the oscillatory OCR_R activity (normalized to ST = 0), with the following parameters: mesor = 1.62 ± 0.11, amplitude = 0.48 ± 0.07, period = 14.42 ± 0.37, acrophase = 11.85 ± 0.47 (Fig. 1B). Even considering the limitation of this experimental model, which does not guarantee long-standing synchronization of the cultured cells, the cosinor analysis would suggest the occurrence of ultradian cycling of the mitochondrial respiration (i.e. with a period lower than 24 h). Notably the rhythmic activity of the mitochondrial respiration resembled closer the oscillatory profile of BMAL1 protein, though postponed by 3 h, rather than that of *BMAL1* mRNA expression (compare with Fig. 1).

Importantly, when the serum-shock protocol was applied to cultured primary human dermal fibroblasts (HDF) or aortic endothelial cells (HAOEC) an almost identical oscillatory OCR was observed in synchronized cells (Figs. S4, S5). Overall these results suggest that the observed autonomous rhythmicity of mitochondrial respiration is a general phenomenon not restricted to a specific cell phenotype.

Mitochondrial respiration generates, under coupled conditions, a trans-membrane electrochemical gradient, provided by outward proton pumping, mainly constituted by electrical potential ($\Delta\Psi_m$) [26].The extent of the OCR_R-related mitochondrial $\Delta\Psi_m$ was assessed by flow-citometry using the $\Delta\Psi_m$-fluorescent probe TMRM. Fig. 2B shows that serum-shocked HepG2 cells resulted in a significantly higher $\Delta\Psi_m$-dependent fluorescence at the synchronization time (ST) = 12 h as compared with that at 6 h and 18 h. Cell imaging by fluorescence microscopy, using the same $\Delta\Psi$-probe, confirmed a significantly higher intracellular signal at the same ST (Fig. 2C). As increased mitochondrial respiratory activity is expected to generate more reactive oxygen species [27] this was assessed flow-citometrically by DCF (a commonly used peroxide-probe). Consistent with the respiratory measurements a significant relative increase of the NAC-sensitive DCF-mediated fluorescence was detectable at ST = 12 h [Fig. S6]. Importantly, treatment of HepG2 cells with the transcription-inhibitor actinomycin D, during synchronization, strongly repressed the rhythmic respiratory activity under conditions suppressing the expression of *BMAL1*, *REV-ERB*α and *ROR*-α (Fig. S7). This latter observation would rule out that the observed respiratory rhythmic activity is independent on transcriptional oscillators as described for other circadian processes [28,29]. The link between the rhythmic mitochondrial respiration and the clock genes was further analyzed in HepG2 cells where the expression of *BMAL1* was specifically inhibited by RNA interference. Fig. 2D,E show that under conditions significantly reducing the expression of *BMAL1* the oscillation of the OCR was completely abrogated in synchronized HepG2 cells.

To verify the extent to which the serum deprivation, included in the serum-shock protocol of synchronization, was somehow accountable for the oscillatory activity of the cell respiration we modified the original protocol replenishing after serum shock the cell with a medium containing 10% serum. As shown in Fig. S8 no significant differences were observed in the rhythmic activity of the OCR in the HepG2 cells synchronized by the two protocols in the 24 h post-synchronization. This result would rule out any appreciable stressing condition of the original protocol [14] affecting mitochondrial respiration in the 24 h timescale post-synchronization.

Cultured HepG2 cells, under non-proliferating conditions, relay for ATP production on the metabolic flux distribution of glucose carbons between glycolysis and pyruvate oxidation [30]. Substitution of glucose with galactose forces cultured cells to rely almost exclusively on mitochondrial OxPhos for ATP production [31]. Fig. 3A shows that synchronized HepG2 cells exhibit a rhythmic respiratory activity also when cultured in the presence of galactose indicating that it occurred independently on the relative contribution of glycolysis. Overall these data suggest that the self-autonomous ultradian rhythmic oscillations of the mitochondrial respiratory activity is irrespective of the respiratory carbon source used.

To assess if the above-described oscillatory activity of mitochondrial respiration was dependent on the specific synchronization protocol used, an alternative procedure was applied consisting in a short-time pre-treatment with dexamethasone [16]. Fig. 3B shows that HepG2 cells exhibited, after withdrawal of dexamethasone, a large-amplitude oscillation of the OCR_R and OCR_U peaking at ST = 12 h. This result ruled out that the observed phasic respiratory activity was related to the condition of serum deprivation demanded after serum load.

To further verify the link between clock genes expression and mitochondrial respiration, serum-shocked HepG2 cells were re-synchronized by dexamethasone treatment. Fig. 3C shows that treatment with dexamethasone before the onset of the expected zenith in serum-shocked HepG2 cells caused a clear shift of the *BMAL1* gene expression, which peaked 6 h later. Remarkably, the OCR_R measured under identical "synchronization-reset-resynchronization" protocol displayed a similar time-shift following dexamethasone treatment. This result strongly indicates a direct functional correlation between the clock-gene machinery and the mitochondrial OxPhos activity.

All together our experimental evidences suggest that in vitro synchronized cultured cells exhibit self-autonomous ultradian rhythmic oscillations of their mitochondrial respiratory activity linked to the expression of the core clock genes. This is a general phenomenon occurring irrespective of *i*) the cell type (i.e. immortalized vs primary cells), *ii*) the respiratory carbon source, and *iii*) the protocol of synchronization.

3.2. The rhythmic respiratory activity of synchronized cells is correlated with the oscillatory expression/activity of NAMPT and SIRT1/3 and with the reversible acetylation state of Complex I

In order to deepen the mechanism controlling the rhythmic mitochondrial respiratory activity we assessed the expression level of the mitochondrial OxPhos complexes. Fig. 4A shows a representative immunoblot carried out with a cocktail of antibodies designed to provide semi-quantitative analysis of the respiratory chain complexes (CI, CII, CIII) and of the H^+-F_1F_0 ATP synthase (CV). The result attained did not show significant changes of any of the OxPhos complexes over time after synchronization. Consistently, the citrate synthase activity, a commonly used marker of mitochondrial mass, did not display any oscillatory pattern in synchronized cells [Fig. 4B]. Intriguingly, and somehow counter-intuitively, the expression level of *PPARGC1A* (encoding for PGC-1α), exhibited a significant oscillatory pattern peaking at ST =

Fig. 2. Analysis of mitochondria-related functions in serum shocked synchronized HepG2 cells. A Measurement of the mitochondrial respiratory activity in intact cells. OCR, oxygen consumption rate; the subscripts "R", "O", "U" refer to resting condition (i.e. endogenous substrate-sustained respiration), respiration in the presence of oligomycin, respiration in the presence of the uncoupler FCCP, respectively. The values were normalized for each run to the respective OCR_R at ST = 0 (actual value 1.65 ± 0.22 nmoles O_2/min/10^6 cells) and then averaged ± S.E.M.; n = 12–16 independent experiments. The cosinor best fits of the OCRs under different conditions is shown as continuous thick lines (see the legend). The OCR_R in the absence of serum shock is also shown; mean ± S.E.M. of n = 4. B Flow cytometric analysis of the $\Delta\Psi_m$, using the fluorescent TMRM probe, shown as normalized integrated mean fluorescence value (i-MFV); mean ± S.E.M. of n = 4; *P < 0.05, **P < 0.01. C Fluorescence microscopy imaging of the $\Delta\Psi_m$ using the fluorescent probe TMRE. Upper panels, representative images compared with the corresponding bright-light optical fields; lower histogram, means of the Fluorescence/cell ± S.E.M. of n = 4; *P < 0.05. D Immunoblotting of BMAL1 in HepG2 cells transfected with *siRNA-BMAL1*. Upper panel: representative Western blotting of mock and siRNA-treated cells at the indicated time post-transfection. Lower histogram: densitometric analysis normalized to β-actin; means ± S.E.M. of n = 3. E Effect of *BMAL1* silencing on the OCR in synchronized HepG2 cells. The OCR_R were normalized to ST = 0 for mock and siRNA-BMAL1 trasfected cells and averaged ± S.E.M. for n = 3 independent preparations; **P < 0.01, mock vs siRNA-treated at the indicated nadir and zenith STs.

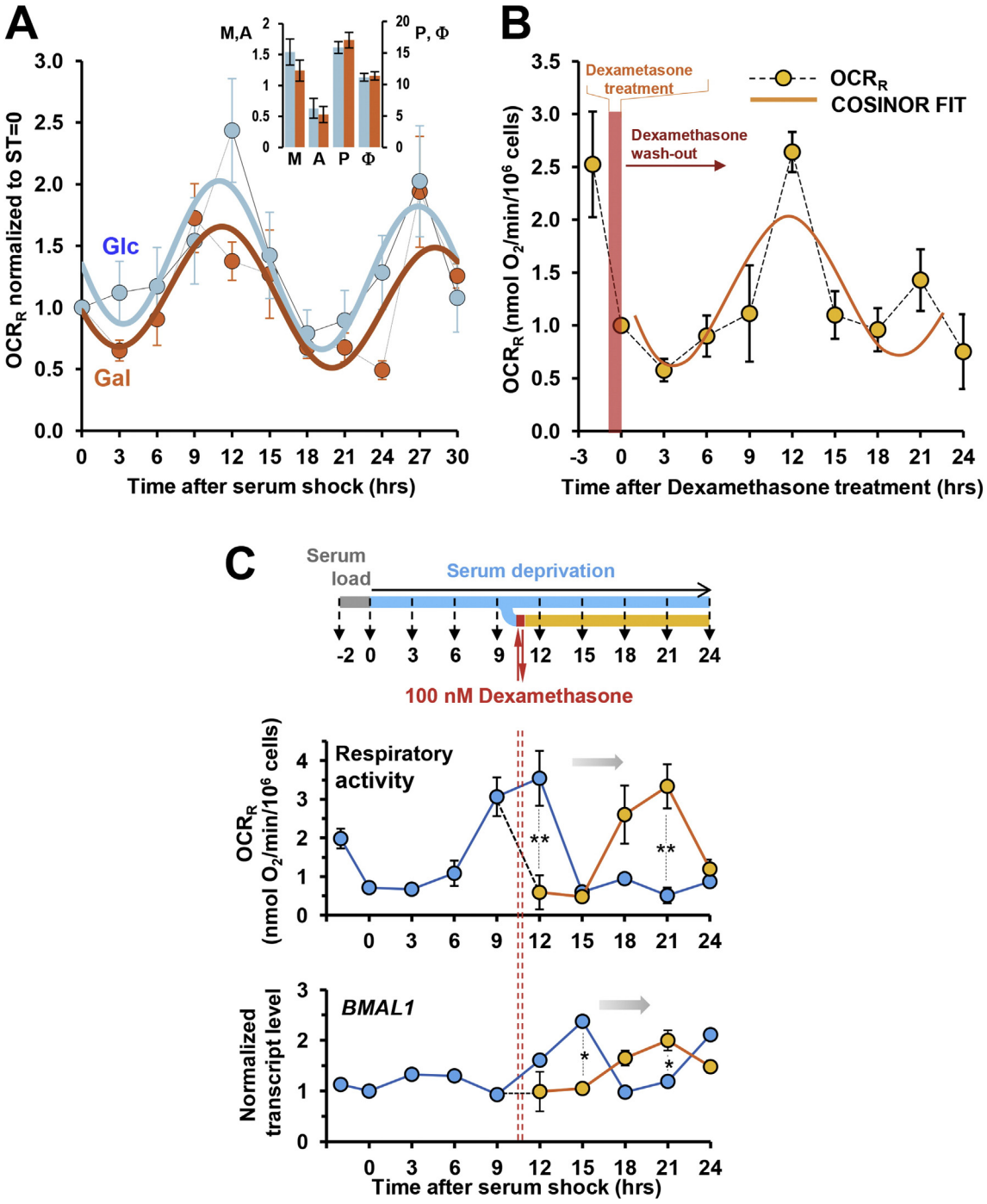

Fig. 3. Effect on mitochondrial respiration of the carbon source in serum-shocked synchronized HepG2 cells and of dexamethasone-mediated synchronization and re-synchronization. A Measurement of the normalized OCR_R in serum-shocked synchronized cells grown in DMEM with galactose (Gal) replacing glucose; for comparison the normalized OCR_R of synchronized cells grown in DMEM with glucose (Glc) run in parallel is also shown; means ± S.E.M. of n = 4; the continuous lines are the cosinor best fits whose parameters are shown in the inset. B Measurement of mitochondrial resting respiratory activity (OCR_R) in dexamethasone-synchronized intact cells; means ± S.E.M. of n = 4. C Serum-shocked cells re-synchronized by dexamethasone treatment. The upper scheme shows the protocol employed; serum shocked cells were treated for 15 min at ST = 11 h with 100 nM dexamethasone and replenished with fresh medium (orange ribbon); dexamethasone-untreated cell served as internal control (light blue ribbon). The upper and lower graphs show the respiratory activity and the expression of *BMAL1* respectively; means ± S.E.M. of n = 3; $^{*}P < 0.05$, $^{**}P < 0.01$.

12 h [Fig. S9]. However, and most notably, PGC-1α proved to stimulate the expression of the clock genes BMAL1 and REV-ERBα, through coactivation of the ROR family of orphan nuclear receptors [32].

A central metabolite controlling the terminal oxidative pathway is represented by NAD [33] and recent reports show that the expression of NAMPT is under control of the clock-gene machinery [7,8]. Accordingly, Fig. 4C shows that the transcript level of the *PBEF1* gene (coding for NAMPT) displayed an oscillatory pattern following synchronization of HepG2 cells with a peak at ST = 12 h. Consistent with this, the total intracellular NAD content significantly increased at about the same time after cell-synchronization as well as the NAD^+/NADH ratio supporting the hypothesis of an enhanced oxidative metabolism at the synchronization time corresponding to the maximal mitochondrial respiratory activity. Importantly, treatment of synchronized cells short before the time preceding the zenith of NAMPT expression (i.e. at ST = 10 h) with FK866, a specific inhibitor of NAMPT, inhibited the rise of

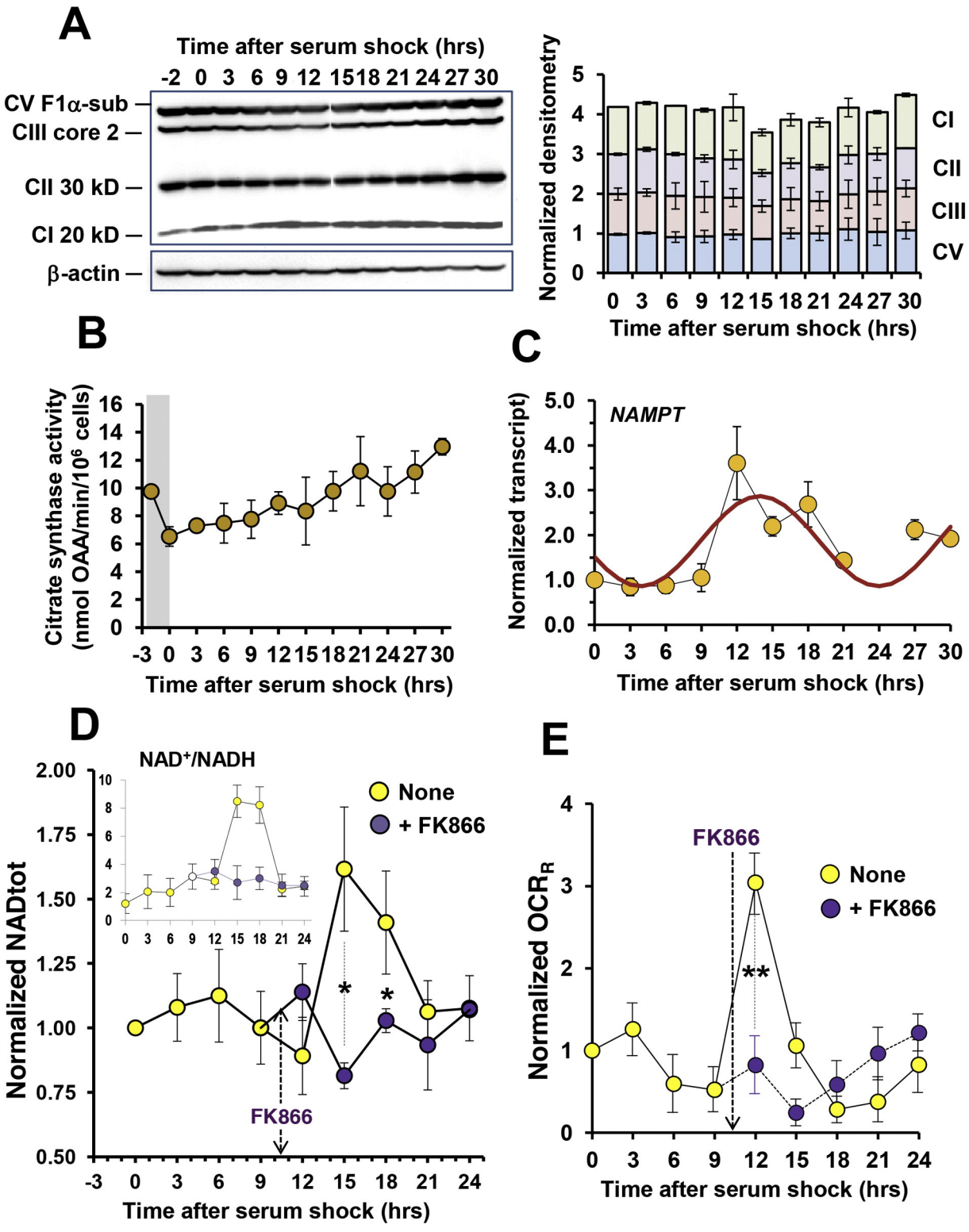

Fig. 4. Analysis of OxPhos complexes, NAMPT expression and NAD level in serum shocked synchronized HepG2 cells. A Mitochondrial OxPhos complexes content. Left panel: representative immunoblotting of total protein extracts with a cocktail of antibodies recognizing the indicated subunits of Complex V (CV, H^+-F_1F_o ATP-synthase), Complex III (CIII, ubiquinol-cytochrome c oxidoreductase), Complex II (CII, succinate dehydrogenase), Complex I (CI, NADH-ubiquinone oxidoreductase). Right panel: normalized densitometric analysis of the OxPhox complexes shown as stacked bar graph; means ± S.E.M. of n = 4. B Citrate synthase activity; means ± S.E.M. of n = 4. C Transcript level of *PBEF1* encoding for NAMPT; the values obtained by qRT-PCR were normalized to ST = 0 h and are means ± S.E.M. of n = 3; the cosinor best fit is shown as continuous line. D Measurement of intracellular total NAD; the absolute values (nmoles/mg proteins) were normalized to ST = 0 and are means ± S.E.M. of n = 4. The inset shows the NAD^+/NADH ratio. Where indicated at ST = 10 h synchronized cells were supplemented with 0.2 μM of the NAMPT inhibitor FK866; means ± S.E.M. of n = 3; *P < 0.05, **P < 0.01. E Effect of FK866 on the mitochondrial resting respiratory activity (OCR_R). Cells were treated with FK866 as in panel (D) (untreated cells served as internal control); means ± s.e.m. of n = 3; **P < 0.01.

NAD content and fully prevented the appearance of the OCR_R-peak [Fig. 4D,E] as well as of the transcription of *BMAL1*, *PBEF1*, *SIRT1*, *SIRT3* at ST = 12 h [Fig. S10].

Next we measured the specific activity of the mitochondrial respiratory chain Complex I (NADH-ubiquinone oxidoreductase) in solubilized HepG2 cells following spectrophotometrically the rate of oxidation of added NADH. Complex I is the main enzymatic step controlling the electron flux through the respiratory chain [34,35]. The results obtained showed that the specific rotenone-sensitive activity of complex I was significantly higher when cells were harvested at ST = 12 as compared with those at ST = 6 and 18 h [Fig. 5A]. Conversely, the succinate-O_2 oxidoreductase activity of the respiratory chain, encompassing the activities of complex II, III and IV, did not exhibit any oscillatory pattern when assayed polarographically in digitonin-permeabilized synchronized HepG2 cells [Fig. 5B]. These results suggested that the increased activity of the mitochondrial respiratory chain, likely controlled by Complex I,

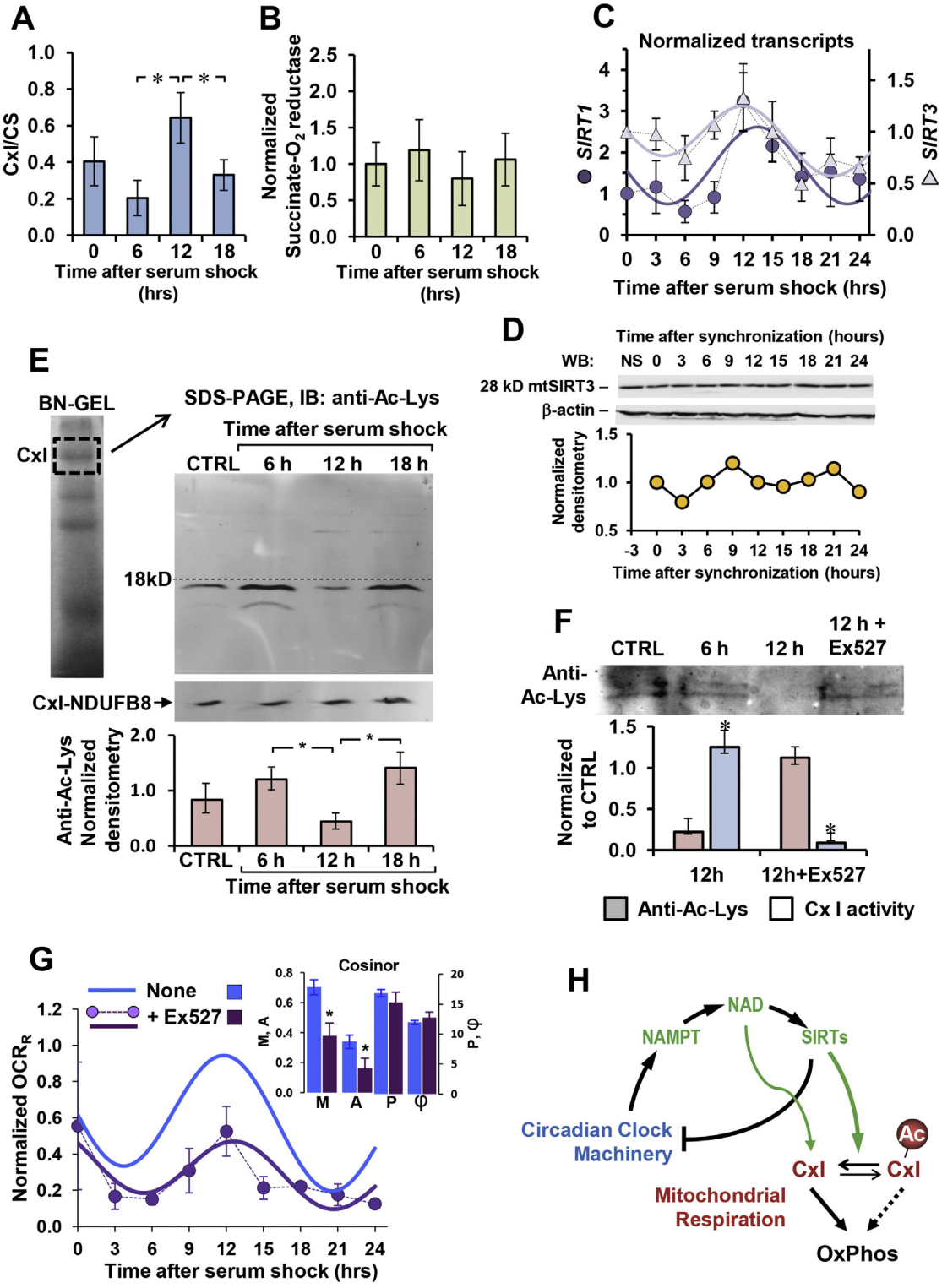

was not directly related to the enhanced availability of NAD as a respiratory substrate, but rather to an intrinsic reversible change of an enzymatic activity.

In addition to accomplish the known function of a redox-coenzyme, connecting glycolysis and the citric acid cycle to OxPhos, NAD is also involved as co-substrate in de-acetylating reactions catalyzed by members of the sirtuins family and for some of these a circadian control of their expression has been reported [36,37]. Fig. 5C confirms that this occurrence ensued also under our experimental conditions showing that the transcript levels of *SIRT1* and the mitochondrial isoform *SIRT3* exhibited an oscillatory profile peaking at ST = 12 h in synchronized HepG2 cells. Immune detection of SIRT3 in total cell protein extract identified the in-mitochondria imported low-molecular weight protein. Following HepG2 cells synchronization, the mitochondrial SIRT3 exhibited a low amplitude oscillation at the border of statistical significance [Fig. 5D].

Activation of sirtuins proved to affect the acetylation state of a number of intra-mitochondrial proteins involved in the terminal metabolism including components of the respiratory chain [38]. To assess this, mitochondria were isolated from synchronized HepG2 cells at selected interval-times, subjected to 2D electrophoresis (blue native (BN) non-denaturating 1st dimension; SDS denaturating 2nd dimension) and blotted with an anti-acetyl-lysine antibody. The 2D-BN-SDS PAGE of solubilized mitochondrial membrane proteins is a well-established procedure to detect all the subunits of the OxPhos complexes (resolved in the first dimension) [19]. A comparison of the outcomes from samples deriving from synchronized cells at ST = 6 h and ST = 12 h, corresponding to the main nadir and zenith of the OCR_R cycle, respectively, revealed the presence of a prominent acetyl-lysine-positive band at ST = 6 h that disappeared almost completely at ZT = 12 h (Fig. S11) and that pointed to a subunit of complex I. SDS-PAGE of complex I excised from BN gels enabled to run in parallel several samples. Fig. 5E shows a representative immuno-blotting confirming that a single subunit of complex I underwent an acetylating-deacetylating cycle that antiphased both the OCR_R and Complex I activities in synchronized HepG2 cells. Most notably, treatment of HepG2 cells with Ex527, a selective sirtuin inhibitor, at the onset of the synchronization protocol, significantly depressed the oscillatory profile of the OCR_R and the relative increase of Complex I activity at ST = 12 h as well as the deacetylated state of its subunit (Figs. 5F,G).

4. Conclusions

The present study supports mounting evidence showing the intertwining between the biological clock and cellular metabolism highlighting in this context the control exerted on the functional property of the mitochondrial respiratory chain and consequently on the OxPhos. The interplay between the clock gene machinery and the NAMPT-NAD-SIRT1/3 axis as a pivotal hub controlling the circadian oscillation of metabolism is here confirmed also in an *in vitro* cellular model. The results here presented strictly show that the oscillating acetylation/deacetylation state of complex I is the solely responsible for the clock-genes-controlled activity of the mitochondrial respiratory chain activity (see the scheme in Fig. 5H), at least under our experimental conditions. It must be pointed out that additional circadian SIRT(s)-mediated activation of catabolic pathway(s), up-stream of the respiratory chain, can contribute to modulate the mitochondrial oxidative performance as clearly shown for the fatty acid β-oxidation [12]. The identification of the specific Complex I subunit undergoing the acetylation/de-acetylation cycle as well as the molecular mechanism controlling the enzymatic activity deserve further investigation. All together our findings provide additional evidence of an interlocked transcriptional-enzymatic feedback loop controlling the molecular interplay between cellular bioenergetics and circadian rhythmicity.

Author contributions

N.C. and G.Ma. generated the ideas and hypotheses, designed all experiments and analyzed data. O.C. and R.S. performed and designed most experiments under supervision of N.C. V.P., G.Me., G.B., B.A., S.F., M.M., R.R. and C.P. participated in experimentation and discussions. A.R. and L.F. designed, generated and analyzed the bioluminescence data. N.C. and G.Ma wrote the manuscript.

Conflict of interest

The authors declare that they have no conflict of interest.

Transparency document.

The Transparency document is associated with this article can be found, in the online version.

Acknowledgments

The authors thank Dr. Giovanni Li Volti, University of Catania, for providing samples of HAOEC and Drs. Martina D'Aronzo and Cristiana Tiberio for participating in the production of some q-RT-PCR data. Financial support: the study was supported to N.C. by local grant of the University of Foggia through the Department of Clinical and Experimental Medicine and to G.Ma. by the "5 × 1000" voluntary contribution and a grant from the Italian Ministry of Health through Division of Internal Medicine and Chronobiology Unit (RC1203ME46, RC1302ME31, RC1403ME50, RC1504ME53), IRCCS "Casa Sollievo della Sofferenza", San Giovanni Rotondo (FG), Italy. A.R. and L.F. were funded by the German Federal Ministry of Education and Research (BMBF)—eBio-CIRSPLICE — FKZ031A316. L.F. was additionally funded by the Berlin School of Integrative Oncology (BSIO) of the Charité Universitätsmedizin Berlin.

Fig. 5. Analysis of Complex I activity and its acetylation state and of OxPhos in serum shocked synchronized HepG2 cells. A Measurement of complex I activity. The complex I activity was measured spectrophotometrically in utrasound-treated cells as rotenone-sensitive initial rate of NADH oxidation (in the presence of UQ_2) and normalized to citrate synthase activity; means ± S.E.M. of n = 4; *P < 0.05. B Measurement of succinate-O_2 reductase activity. Digitonin-permeabilized cells were supplemented with succinate and assessed by respirometry in the presence of rotenone; the OCR was corrected for residual activity in the presence of antimycin A and normalized to ST = 0; means ± S.E.M. of n = 3. C Transcript level of *SIRT1* and *SIRT3*; the values obtained by qRT-PCR were normalized to ST = 0 h and are means ± S.E.M. of n = 3; the cosinor best fits are shown as continuous lines. D Immunoblotting of SIRT3 on total protein extract. Top panel: representative Western blotting showing the mitochondria-localized 28 kD form of the protein. Lower graph: densitometry of the SIRT3 band normalized to b-actin and to ST = 0 h; average of 2 independent experiments resulting in comparable outcome. E Representative immunoblotting of complex I with antibody recognizing acetylated lysine. Mitochondria enriched fractions were isolated in the presence of 5 μM of the SIRTs inhibitor Ex527 from serum-shocked HepG2 cells at the indicated ST (non synchronized cells were also processed - CTRL) and subjected to blue native (BN) electrophoresis under non denaturating condition (a representative result is shown). Thereafter the bands corresponding to complex I were excised, subjected to electrophoresis under denaturating conditions and Western blotted (as protein loaded control the blot was stripped and treated with an Ab recognizing the 18 kD complex I subunit NDUFB8). Bottom panel: normalized densitometric analysis of acetylated band; means ± S.E.M. of n = 3; *P < 0.05. F Effect of Ex527 on the acetylation state and activity of Complex I. Cells were treated with 5 μM Ex527 at the onset of serum-shock synchronization and analyzed at ST = 12 h (non-synchronized and untreated cells served as control). Upper panel: representative immunoblotting with anti-Ac-Lys Ab obtained as in panel (D). Bottom panel: normalized densitometric analysis and Complex I activity at ST = 12 h of untreated and Ex527-treated cells; means ± S.E.M. of n = 3; *P < 0.01. G Effect of Ex527 on resting respiratory activity; means ± S.E.M. of n = 3. The cosinor best fit of treated cells is shown as continuous line; for comparison the cosinor best fit of untreated cells and the cosinor parameters (in the inset) are also shown; *P < 0.05. H Scheme showing the interlocked transcriptional-enzymatic feedback loop controlling the molecular interplay between cellular bioenergetics and circadian rhythmicity as inferred from the present study.

Appendix A. Supplementary data

Supplementary data to this article can be found online at http://dx.doi.org/10.1016/j.bbamcr.2015.12.018.

References

[1] C. Dibner, U. Schibler, U. Albrecht, The mammalian circadian timing system: organization and coordination of central and peripheral clocks, Annu. Rev. Physiol. 72 (2010) 517–549.
[2] J.S. Takahashi, H.K. Hong, C.H. Ko, E.L. McDearmon, The genetics of mammalian circadian order and disorder: implications for physiology and disease, Nat. Rev. Genet. 9 (2008) 764–775.
[3] N. Preitner, et al., The orphan nuclear receptor REV-ERBalpha controls circadian transcription within the positive limb of the mammalian circadian oscillator, Cell 110 (2002) 251–260.
[4] U. Albrecht, Timing to perfection: the biology of central and peripheral circadian clocks, Neuron 74 (2012) 246–260.
[5] R. Zhang, N.F. Lahens, H.I. Balance, M.E. Hughes, J.B. Hogenesch, A circadian gene expression atlas in mammals: implications for biology and medicine, Proc. Natl. Acad. Sci. U. S. A. 111 (2014) 16219–16224.
[6] G. Asher, et al., SIRT1 regulates circadian clock gene expression through PER2 deacetylation, Cell 134 (2008) 317–328.
[7] Y. Nakahata, S. Sahar, G. Astarita, M. Kaluzova, P. Sassone-Corsi, Circadian control of the NAD+ salvage pathway by CLOCK-SIRT1, Science 324 (2009) 654–657.
[8] K.M. Ramsey, et al., Circadian clock feedback cycle through NAMPT-mediated NAD+ biosynthesis, Science 324 (2009) 651–654.
[9] B.M. Spiegelman, Transcriptional control of mitochondrial energy metabolism through the PGC1 coactivators, Novartis Found. Symp. 287 (2007) 60–63.
[10] J. Bass, J.S. Takahashi, Circadian integration of metabolism and energetics, Science 330 (2010) 1349–1354.
[11] J. Bass, Circadian topology of metabolism, Nature 491 (2012) 348–356.
[12] C.B. Peek, et al., Circadian clock NAD+ cycle drives mitochondrial oxidative metabolism in mice, Science 342 (2013) 1243417.
[13] D. Jacobi, et al., Hepatic Bmal1 regulates rhythmic mitochondrial dynamics and promotes metabolic fitness, Cell Metab. 22 (2015) 709–720.
[14] A. Balsalobre, F. Damiola, U. Schibler, A serum shock induces circadian gene expression in mammalian tissue culture cells, Cell 93 (1998) 929–937.
[15] G. Benegiamo, et al., Mutual antagonism between circadian protein period 2 and hepatitis C virus replication in hepatocytes, PLoS One 8 (2013), e60527.
[16] A. Balsalobre, et al., Resetting of circadian time in peripheral tissues by glucocorticoid signaling, Science 289 (2000) 2344–2347.
[17] S.A. Brown, F. Fleury-Olela, E. Nagoshi, C. Hauser, C. Juge, et al., The period length of fibroblast circadian gene expression varies widely among human individuals, PLoS Biol. 3 (2005), e338.
[18] A. Barrientos, F. Fontanesi, F. Díaz, Evaluation of the mitochondrial respiratory chain and oxidative phosphorylation system using polarography and spectrophotometric enzyme assays, Curr. Protoc. Hum. Genet. (2009) Chapter 19, Unit19.3.
[19] H. Schägger, K. Pfeiffer, The ratio of oxidative phosphorylation complexes I–V in bovine heart mitochondria and the composition of respiratory chain supercomplexes, J. Biol. Chem. 276 (2001) 37861–37867.
[20] M. Pinti, et al., Hepatoma HepG2 cells as a model for in vitro studies on mitochondrial toxicity of antiviral drugs: which correlation with the patient? J. Biol. Regul. Homeost. Agents 17 (2003) 166–171.
[21] E.L. McDearmon, et al., Dissecting the functions of the mammalian clock protein BMAL1 by tissue-specific rescue in mice, Science 314 (2006) 1304–1308.
[22] G. Cornelissen, Cosinor-based rhythmometry, Theor. Biol. Med. Model. 11 (2014) 16.
[23] E. Nagoshi, S.A. Brown, C. Dibner, B. Kornmann, U. Schibler, Circadian gene expression in cultured cells, Methods Enzymol. 393 (2005) 543–557.
[24] T. Tamaru, et al., Hirayama J, isojima Y, Nagai K, Norioka S, Takamatsu K, Sassone-Corsi P. CK2alpha phosphorylates BMAL1 to regulate the mammalian clock, Nat. Struct. Mol. Biol. 16 (2009) 446–448.
[25] Y. Lee, E.K. Kim, AMP-activated protein kinase as a key molecular link between metabolism and clockwork, Exp. Mol. Med. 45 (2013), e33.
[26] D.G. Nicholls, S.J. Ferguson, Bioenergetics4, Academic Press, New York, 2014.
[27] R.J. Mailloux, Teaching the fundamentals of electron transfer reactions in mitochondria and the production and detection of reactive oxygen species, Redox Biol. 4C (2015) 381–398.
[28] A.B. Reddy, G. Rey, Metabolic and nontranscriptional circadian clocks: eukaryotes, Annu. Rev. Biochem. 83 (2014) 165–189.
[29] S. Kojima, C.B. Green, Circadian genomics reveal a role for post-transcriptional regulation in mammals, Biochemistry 54 (2015) 124–133.
[30] D.A. Ouattara, et al., Metabolomics-on-a-chip and metabolic flux analysis for label-free modeling of the internal metabolism of HepG2/C3A cells, Mol. BioSyst. 8 (2012) 1908–1920.
[31] R. Rossignol, et al., Energy substrate modulates mitochondrial structure and oxidative capacity in cancer cells, Cancer Res. 64 (2004) 985–993.
[32] C. Liu, S. Li, T. Liu, J. Borjigin, J.D. Lin, Transcriptional coactivator PGC-1alpha integrates the mammalian clock and energy metabolism, Nature 447 (2007) 477–481.
[33] L. Mouchiroud, R.H. Houtkooper, J. Auwerx, NAD^+ metabolism: a therapeutic target for age-related metabolic disease, Crit. Rev. Biochem. Mol. Biol. 48 (2013) 397–408.
[34] U. Brandt, Energy converting NADH:quinone oxidoreductase (complex I), Annu. Rev. Biochem. 75 (2006) 69–92.
[35] G. Quarato, C. Piccoli, R. Scrima, N. Capitanio, Variation of flux control coefficient of cytochrome c oxidase and of the other respiratory chain complexes at different values of protonmotive force occurs by a threshold mechanism, Biochim. Biophys. Acta 1807 (2011) 1114–11124.
[36] H.C. Chang, L. Guarente, SIRT1 and other sirtuins in metabolism, Trends Endocrinol. Metab. 25 (2014) 138–145.
[37] S. Masri, P. Sassone-Corsi, Sirtuins and the circadian clock: bridging chromatin and metabolism, Sci. Signal. 7 (2014) re6.
[38] F.M. Amado, A. Barros, A.L. Azevedo, R. Vitorino, R. Ferreira, An integrated perspective and functional impact of the mitochondrial acetylome, Expert Rev. Proteomics 11 (2014) 383–394.